IEEE Access
Multidisciplinary | Rapid Review | Open Access Journal

Received July 10, 2020, accepted July 28, 2020, date of publication July 30, 2020, date of current version August 11, 2020.

Digital Object Identifier 10.1109/ACCESS.2020.3013140

Isolated Ground-Radiation Antenna With Inherent Decoupling Effect and Its Applications in 5G MIMO Antenna Array

HAIYAN PIAO[1], YUNNAN JIN[1], (Member, IEEE), AND LONGYUE QU[1,2], (Member, IEEE)
[1]Department of Electronics and Computer Engineering, Hanyang University, Seoul 04763, South Korea
[2]School of Electronics and Information Engineering, Nanjing University of Information Science and Technology (NUIST), Nanjing 210000, China

Corresponding author: Longyue Qu (rioinkorea@gmail.com)

This work was supported in part by the China Scholarship Council (CSC), and in part by the Hanyang Antenna Company Ltd., Shenzhen, China.

ABSTRACT This paper studies an isolated ground-radiation antenna (iGradiANT) that has inherent isolation with another closely-located antenna element and demonstrates its applications in 5G multiple-input multiple-output (MIMO) antenna array. The proposed iGradiANT is accomplished by merely employing a small out-of-ground loop into a traditional ground-radiation antenna (GradiANT). Hence, in contrast to the traditional GradiANT, the proposed iGradiANT can simultaneously support an in-ground loop-type current mode and an out-of-ground loop-type current mode, responsible for far-field radiation and near-field energy cancellation, respectively. In this way, the proposed iGradiANT can exhibit an intrinsic decoupling effect with the adjacent antenna element. Hereby, a typically used inverted-F antenna (IFA) and a normal loop antenna are adopted to separately validate the functionality and versatility of the proposed iGradiANT in establishing 2 × 2 MIMO antenna sets without any separation. Furthermore, an 8 × 8 MIMO antenna array is demonstrated for the usage of 5G terminal devices; both simulation and measurement are conducted to verify its radiation performance and diversity performance.

INDEX TERMS Isolated ground-radiation antenna (iGradiANT), inherent isolation, 5G, multiple-input multiple-output (MIMO), terminal devices.

I. INTRODUCTION

With the explosion of the user number and a burst of powerful cellular devices, there is a tremendous demand for fast data rates. The next-generation communication (5G) is proposed to address this demand by employing the unprecedented spectrum of sub-6 GHz band and millimeter wave (mmWave) band, such that characteristics of ultra-fast speeds, low latency, and excellent reliability, can be supported [1], [2]. In the sub-6 GHz layer, the allocation of the 3.5 GHz band (3.4–3.6 GHz) for 5G wireless communication [3] has brought an explosion of ground-breaking research works in multiple-input multiple-output (MIMO) antenna systems for current and future terminal devices [4]–[32]. It has been proved that the integration of more antenna elements into terminal devices can significantly increase energy efficiency, spectral efficiency, robustness, and reliability, thus satisfying the growing demands of 5G wireless communication.

It is of such great interest yet a significant challenge to design MIMO antenna systems with high integration, miniaturized volume, low interference, and low correlation; this is especially true in terminal devices due to size limitation and placement constraint. In the literature, the most recent studies focused on the realization of self-decoupled compact MIMO antenna sets using polarization or pattern control and on their duplication for the sake of N × N MIMO arrays [4]–[15]; otherwise, other research investigated decoupled MIMO antenna arrays by introducing decoupling structures [16]–[22], while the rest relies on the spatial distance to realize optimized arrangement of the MIMO antenna arrays [23]–[30]. These methods usually suffer from complicated installment, massive structures, or relatively large separations between antenna elements. Moreover, 3 × 3 or 4 × 4 MIMO antenna sets are also proposed [31], [32], having

The associate editor coordinating the review of this manuscript and approving it for publication was Chinmoy Saha.

higher integration but at the cost of increased implementation complexity.

More importantly, most of the adopted methods in the reported MIMO antenna arrays are not new, and they were systematically investigated years ago for 4G Long-Term Evolution (LTE) applications, including decoupling circuits [33]–[37], neutralization lines [38]–[42], parasitic elements [43]–[47], and mode/polarization control [48]–[53]. Thereinto, the decoupling circuits usually require many lumped elements and occupy large circuit area, which may increase the implementation difficulty and degrade the radiation performance (low radiation efficiency and narrow impedance bandwidth). The neutralization lines can only be applied in specified cases and for limited antenna types, whereas the parasitic elements usually suffer from large occupation due to the additionally introduced structures. As for the last method, most terminal devices can only support a few modes or polarizations, limiting the integration scale of antennas. Additionally, the typically adopted antenna types in the literature are confined to inverted-F antennas (IFAs), monopole antennas, patch antennas, half-wavelength loop antennas, and quarter-wavelength open-slot antennas; thus, large volumes are occupied by the antenna elements, which further increases the implementation difficulty and fabrication cost.

In contrast to the antenna types mentioned above, the ground-radiation antenna (GradiANT) [54]–[62] has attracted considerable attention due to its valued features in compactness, tunability, easy fabrication, low cost, and high radiation performance. It is a loop-type resonator occupying a small clearance, such that it is strongly coupled to the ground plane for radiation. Although this kind of antenna has been popularly applied in terminal devices, most previously reported GradiANTs focused on single antenna elements. Several MIMO antennas have been studied [57], [59], but their distances are enormous, which apparently can no longer satisfy the increasing request for N × N MIMO arrays. More importantly, even though the decoupling techniques mentioned above (e.g., decoupling circuits, neutralization lines, mode/polarization control) are well-known ones, unfortunately, there is no evidence to suggest they can be duplicated into GradiANTs. This motivates this paper to derive a new decoupling method that is suitable for GradiANTs and to accomplish a compact MIMO antenna array so that they can be applied to current and future 5G terminal devices.

In this paper, an isolated ground-radiation antenna (iGradiANT) with an inherent decoupling effect with another antenna element is reported in the first of its kind [63]. The proposed iGradiANT is accomplished by assembling a simple out-of-ground loop into a conventional GradiANT, such that an in-ground loop-type current mode for far-field radiation and an out-of-ground loop-type current mode for anti-phase cancellation are simultaneously excited. In this way, the near-field electromagnetic coupling from the iGradiANT to another antenna element can be dramatically mitigated. Herein, a typically used IFA is selected to integrate with iGradiANT and construct an integrated MIMO antenna set, and a normal loop antenna is also investigated to verify the versatility of the proposed iGradiANT.

Different from the decoupling mechanism reported in [4]–[53], the proposed iGradiANT is evolved from a conventional GradiANT, thereby acquiring inherent decoupling capability with another antenna element, so that it can operate as a versatile technique to construct integrated MIMO antenna sets. Such a MIMO antenna technique is proposed for the first time. Besides, the proposed iGradiANT allows the accomplishment of totally integrated MIMO antenna sets without any separation or distance between the iGradiANT and another antenna element, addressing the desperate demand for compact MIMO antenna sets in terminals.

The rest of this paper is organized as follows. In Section II, the basic configuration of the iGradiANT is described, and its fundamental characteristics are explained. In Section III, an integrated 2 × 2 MIMO antenna set without any separation is designed by combining an IFA with the iGradiANT. A compact design is further discussed to address the key challenge in volume constraint, and the integration method with a normal loop antenna is also presented to demonstrate the feasibility and versatility of the proposed technique. In Section IV, an 8 × 8 MIMO antenna array is demonstrated, and its simulation and measurement results were conducted to validate the practicability of the proposed MIMO antenna system for 5G applications.

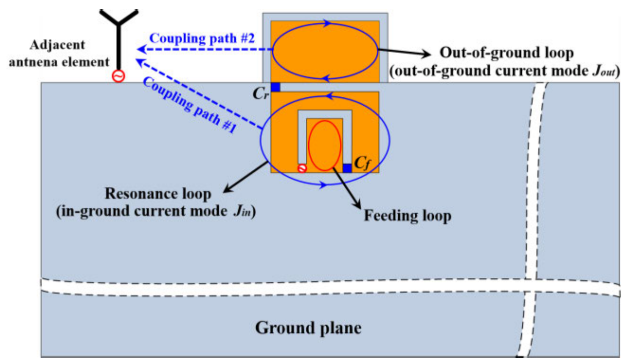

FIGURE 1. Schematic diagram of the iGradiANT for MIMO antennas.

II. ISOLATED GROUND-RADIATION ANTENNA

Figure 1 depicts the configuration of the proposed iGradiANT, which is comprised of a feeding loop, a resonance loop, and an out-of-ground loop. The feeding loop consisting of a feeding capacitor C_f and the resonance loop consisting of a resonance capacitor C_r are responsible for the impedance matching and resonance control, respectively, which also constitute the basic structural features of a traditional GradiANT. The significant difference between a traditional GradiANT and the proposed iGradiANT lies in the employment of the out-of-ground loop that encloses the resonance capacitor C_r. More specifically, the iGradiANT can simultaneously support an in-ground loop-type current mode ($\boldsymbol{J}_{in}$) around the resonance loop and an out-of-ground loop-type current mode ($\boldsymbol{J}_{out}$) around the out-of-ground loop.

Similar to the traditional GradiANT, the capacitor C_r is loaded as an external capacitance component to the antenna, so that the antenna's resonant frequency can be decreased only by increasing the capacitor value of C_r without modifying the antenna's dimensions. Meanwhile, the impedance matching is determined by the mutual coupling between the feeding loop and the resonance loop, which can be easily controlled by adjusting the capacitor value of C_f. In this way, both the resonant frequency and the impedance matching of the iGradiANT can be optimized by choosing proper capacitor values of C_r and C_f, respectively. In. Detailed information on the controlling principle can be found by referring to [54], [62]. Although distributed capacitive structures (e.g., interdigital structures) can also provide desired capacitance, lumped elements are preferred because of their advantages in tunability, small volume, easy integration, high-Q factor (i.e., low ohmic loss), especially in practical applications.

As shown in Fig. 1, the in-ground loop-type current mode ($\boldsymbol{J}_{in}$) is formed around the resonance loop and by utilizing the inductance from the ground plane. Alternatively, the out-of-ground loop-type current mode ($\boldsymbol{J}_{out}$) can be observed around the out-of-ground loop but with a reverse direction with respect to the in-ground current mode ($\boldsymbol{J}_{in}$). Both the in-ground loop-type current mode ($\boldsymbol{J}_{in}$) and the anti-phase out-of-ground loop-type current mode ($\boldsymbol{J}_{out}$) flow through the resonance capacitor C_r together. Accordingly, there are two coupling paths from the iGradiANT to the adjacent antenna element, and these two coupling paths may cancel with each other due to opposite phases. This fact allows the iGradiANT to exhibit inherent isolation with another antenna element and to suit for MIMO applications, which is an exciting feature that is not reported in the literature. Hereinafter, MIMO antennas are discussed by investigating the integration methods of the proposed iGradiANT with two different types of normally used antennas (an IFA and a loop antenna) with an emphasis on the most frequently used IFA. A comprehensive investigation is discussed in the following sections.

It is important to note that the in-ground current mode ($\boldsymbol{J}_{in}$) can be widely spread to the ground plane, dominantly contributing to the far-field radiation by operating as an inductive coupling element to the ground plane and by exciting the ground plane as a real radiator [54]–[62]. Otherwise, the out-of-ground current mode ($\boldsymbol{J}_{out}$) is restricted outside of the ground plane and has weak coupling with the ground plane, only operating as a build-in decoupling element to the adjacent antenna element through near-field energy cancellation. For this reason, the out-of-ground loop barely affects the radiation pattern of iGradiANT when compared to a traditional GradiANT, and this fact has been confirmed in simulation.

III. ISOLATED GROUND-RADIATION ANTENNA

A. ANTENNA CONFIGURATION

Based on the proposed technique described in Section II, an integrated 2 × 2 MIMO antenna set is accomplished by combining a typically used IFA with the iGradiANT.

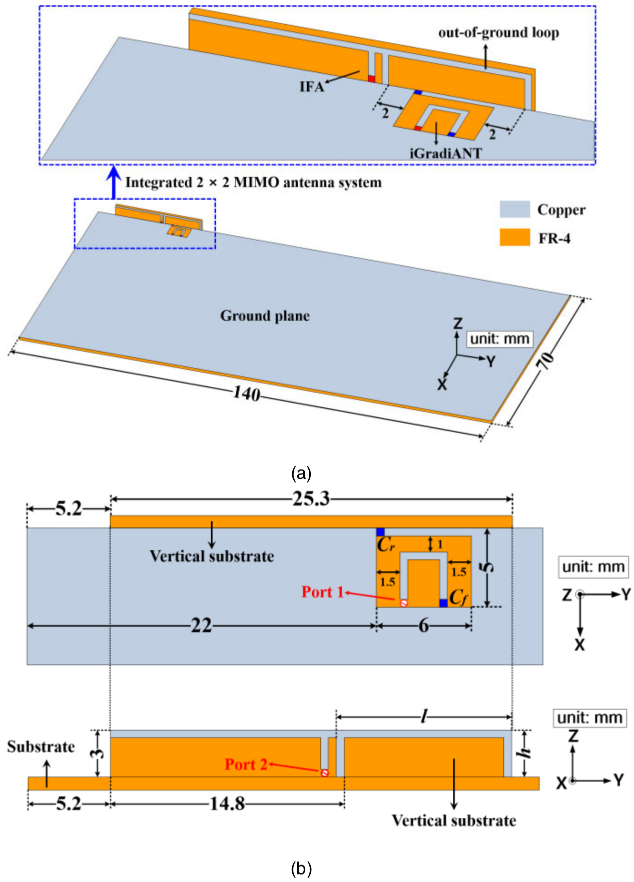

FIGURE 2. Antenna configurations of the proposed integrated MIMO antenna set: (a) perspective view, and (b) side view.

As depicted in Fig. 2, the resonance loop and the feeding loop of the iGradiANT are designed within a small clearance (5 mm × 6 mm) of a 140 mm × 70 mm ground plane, which is etched in a 0.8-mm-thick FR4 substrate ($\varepsilon_r = 4.4$, tan $\delta = 0.02$). The resonance capacitor C_r (0.13 pF) and the feeding capacitor C_f (0.12 pF) are adopted for convenient control of the resonant frequency and impedance matching, respectively. The out-of-ground loop of the iGradiANT, having a length l (11 mm) and a height h (3 mm), is vertically implemented and etched in a 0.8-mm-thick FR4 substrate.

Here, a typically used IFA is introduced in the vicinity of the iGradiANT by sharing part of the out-of-ground loop; thus, the IFA and the iGradiANT are integrated without any separation. Both the IFA and out-of-ground loop are etched in the same 0.8-mm-thick FR4 substrate for the sake of easy fabrication. The IFA has a simple structure and occupies an area of 3 mm × 14.8 mm, so the overall dimension of the vertically implemented FR4 substrate is 3 mm × 25.3 mm × 0.8 mm. Note that the width of all conductor lines is 0.5 mm, and more information can be referred to in Fig. 2. For comparison, the reference MIMO antenna set is designated as the one without the out-of-ground loop, i.e., the combination of the IFA and the conventional GradiANT, which is not shown here for simplicity.

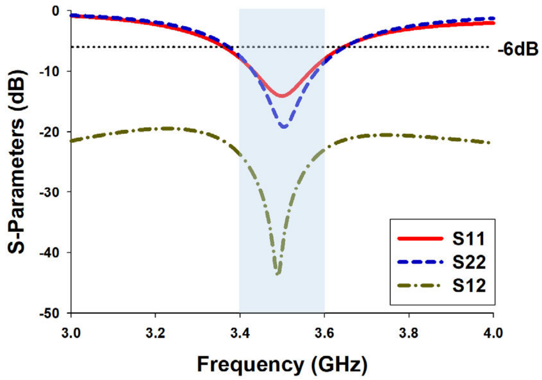

(a)

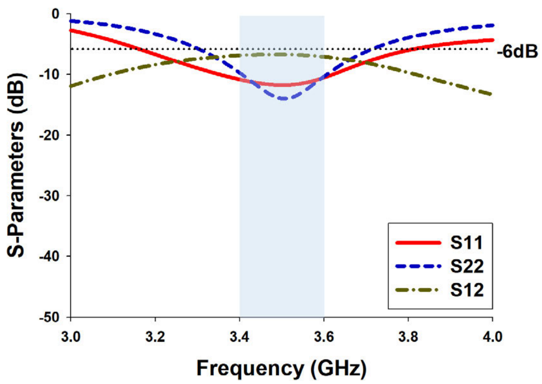

(b)

FIGURE 3. Simulated S-parameters: (a) the proposed integrated MIMO antenna set, and (b) the reference MIMO antenna set.

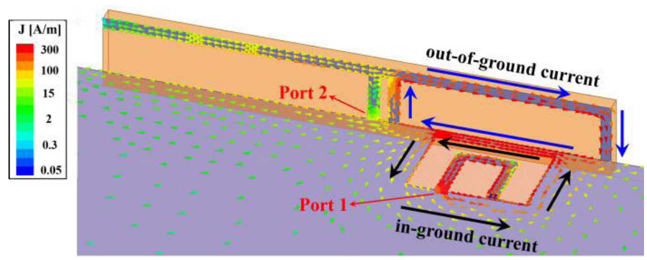

(a)

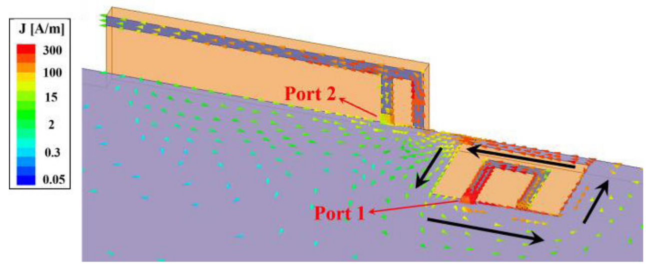

(b)

FIGURE 4. Simulated surface current distributions: (a) the proposed integrated MIMO antenna set with excitation of the iGradiANT at 3.5 GHz, and (b) the reference MIMO antenna set with excitation of the traditional GradiANT at 3.5 GHz.

Figure 3(a) presents the simulated scattering parameters (S-parameters) of the proposed integrated MIMO antenna set. As shown, both the iGradiANT and the IFA operate at the 3.5 GHz target frequency band, and their 3:1 VSWR bandwidths are 280 MHz (from 3.36 to 3.64 GHz) and 270 MHz (from 3.37 to 3.64 GHz), respectively. It is noted that the 3:1 VSWR bandwidth is totally sufficient to evaluate the impedance bandwidth characteristic, as reported in previous literature [5], [9], [11]–[13]. In the S_{12} curve, a coupling null can be observed within the operating frequency band, thereby producing very high isolation above 23 dB with a peak value of 44 dB. For comparison, the S-parameters of the reference MIMO antenna set without the out-of-ground loop is presented in Fig. 3(b), where severe mutual coupling (as high as −6.5 dB) can be observed, indicating that inherent isolation does not exist between the IFA and the traditional GradiANT. It is noted that wider impedance bandwidths in Fig. 3(b) are dominantly attributed to the strong coupled power from one port to another. Therefore, the proposed integrated MIMO antenna set can produce sufficient bandwidth and extremely low mutual coupling, indicating the functionality of the proposed iGradiANT.

To better understand the operation mechanism of the proposed iGradiANT, the simulated surface current distributions of the proposed integrated MIMO antenna set at 3.5 GHz are plotted in Fig. 4. As expected and shown, the in-ground current mode is excited by the feeding loop, and it flows around the resonance loop, such that the antenna can operate as a magnetic coupling element to excite the ground plane as a radiator for far-field radiation. In contrast, the out-of-ground current mode has a reverse current flow around the out-of-ground loop (see Fig. 4(a)). This current distribution ensures the fundamental characteristic (inherent isolation with the adjacent IFA) of iGradiANT. Consequently, extremely weak current flow is inducted into the IFA. On the contrary, strong induced currents are flowing into the IFA when the out-of-ground loop is not implemented (see Fig. 4(b)), and this is the case because the traditional GradiANT and the IFA are tightly arranged and strongly coupled with each other.

B. PARAMETER STUDY

According to the proposed technique, the anti-phase out-of-ground current mode (J_{out}) is of importance to support inherent isolation with the adjacent IFA, so some essential parameters regarding the out-of-ground loop (the length l, the height h, and the resonance capacitor C_r) are investigated in this subsection. It is noted that the reflection coefficients of the IFA are omitted because they are barely affected by the modification of the above parameters.

To start, the length l of the out-of-ground loop is discussed to verify its isolating effect between the iGradiANT and the IFA. The results are derived by manipulating l while retuning the values of C_r and C_f to maintain optimized results. As shown in Fig. 5, the coupling null in the S_{12} curves shifts to a lower frequency band (from 3.7 to 3.3 GHz) as l increases from 9 to 13 mm. This is because the operating frequency of the out-of-ground current mode (J_{out}) varies with the

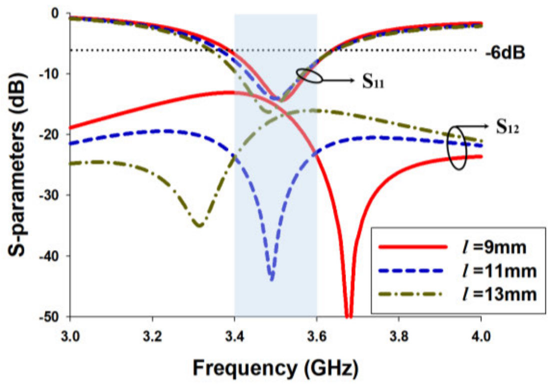

FIGURE 5. Simulated S-parameters with the variation of the length l of the out-of-ground loop.

modification of the dimension of the out-of-ground loop; in this way, optimized isolation can be obtained. Besides, it can be observed from the S_{11} curves that the impedance bandwidth of the iGradiANT slightly degrades as the length l decreases.

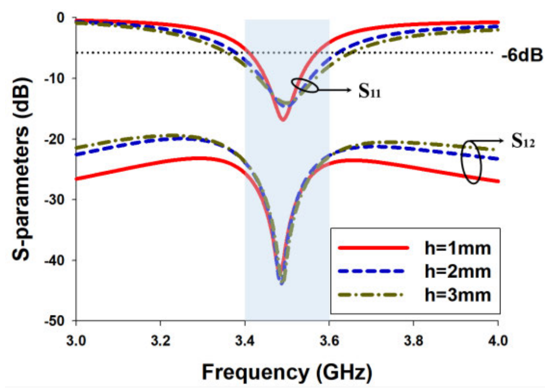

FIGURE 6. Simulated S-parameters with the variation of the height h of the out-of-ground loop.

Next, the height h of the out-of-ground loop is studied in Fig. 6, where the data are derived by modifying the height h while re-adjusting other parameters (l, C_r, and C_f) for optimized results. As can be observed from the S_{12} curves, high isolation properties can be guaranteed in all cases due to the produced decoupling nulls. In the S_{11} curves, however, the impedance bandwidth of the iGradiANT degrades as the height h decreases. With reference to Figs. 5 and 6, a smaller dimension (both the length l and the height h) of the out-of-ground loop may degrade the radiation performance of the iGradiANT.

Since the resonance loop and the out-of-ground loop shares the resonance capacitor C_r, it is expected that the value of C_r can simultaneously determine the operating frequencies of the out-of-ground current mode and in-ground current mode, *i.e.*, the coupling null and the antenna's resonant frequency. As shown in Fig. 7, an increased value of C_r lowers down the resonant frequency of the iGradiANT (see S_{11} curves) and the operating frequency of the coupling null (see S_{12} curves). With reference to Fig. 5 and Fig. 7, the coupling null can be dominantly controlled by modifying the length l of the out-of-ground loop, and the antenna's resonant frequency can be dominantly controlled by adjusting the value of the resonance capacitor (C_r).

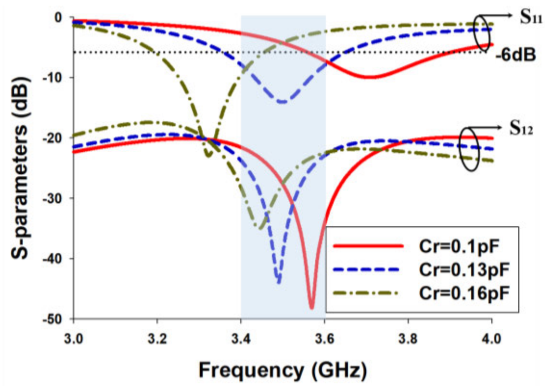

FIGURE 7. Simulated S-parameters with the variation of the capacitor value C_r.

C. FURTHER STUDY AND DISCUSSION

1) COMPACT DESIGN

Here, the compact design of the proposed integrated 2 × 2 MIMO antenna set is presented, where a more compact iGradiANT method is displayed in Fig. 8. As can be observed, only a 1 mm-wide L-shaped ground clearance is occupied so that less ground clearance is required in the ground plane, whereas the dimension of the out-of-ground loop is substantially reduced from 3 mm × 11 mm to 3 mm × 4 mm by loading an inductor element L. The inductor element L can effectively increase the electrical length of the out-of-ground loop and control the out-of-ground current mode without modifying its physical dimensions. In this case, the values of C_r, C_f, and L are 0.25 pF, 0.3 pF, and 4.7 nH, respectively. It is noted that the dimension of the IFA is the same as that in Fig. 1. Figure 8(c) displays the simulated S-parameters of the compact design of the proposed MIMO antenna set, and it can be seen that the compact design can generate similar results to those in Fig.2(a). Additionally, there are various miniaturization methods to achieve more compact designs of both the IFA and iGradiANT such that the proposed MIMO antenna set can be fit into various terminal devices by addressing the key challenges in compactness, which is not further discussed here.

2) INTEGRATION OF IGRADANT AND LOOP ANTENNA

The integration method of the iGradiANT with a normally used IFA has been described hereinbefore. In his subsection, the iGradiANT is integrated with a normal loop antenna to validate the versatility of the proposed technique, as depicted in Fig. 9.

For the iGradiANT, the ground clearance and the capacitor values are the same as those in Fig. 1, whereas the dimension of the out-of-ground loop is adjusted as 3 mm × 12 mm for optimized isolation performance. A loop antenna is installed in the vicinity of the iGradiANT and directly connected with the out-of-ground loop; in such way, the loop antenna

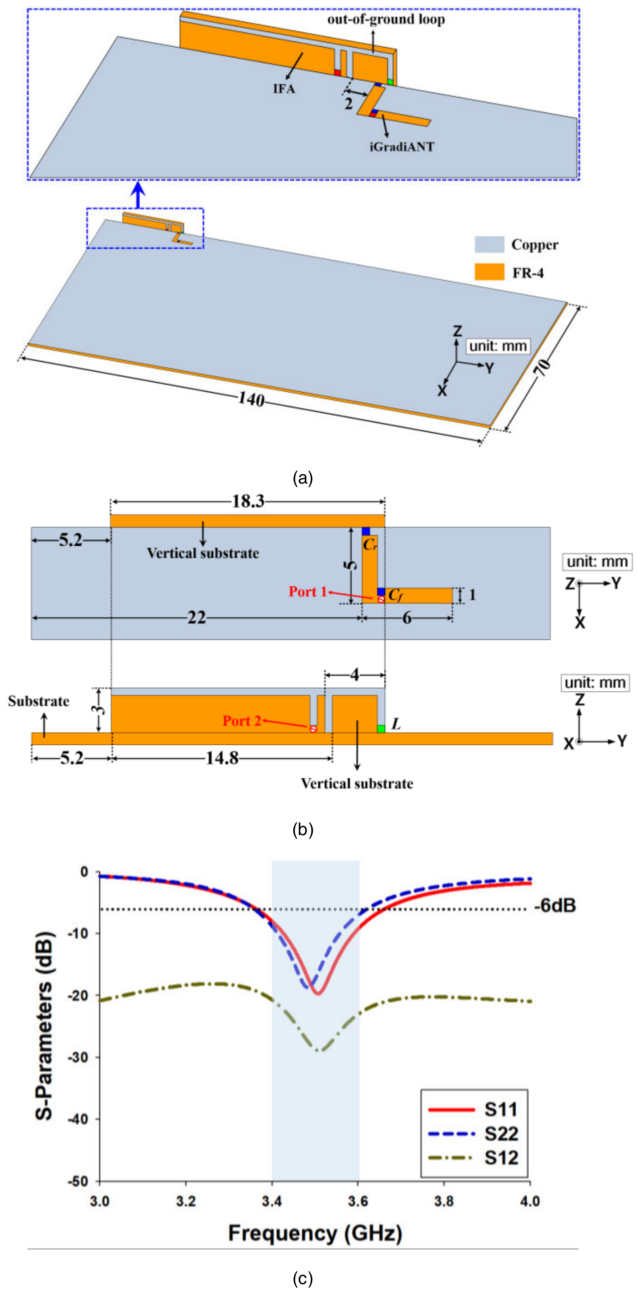

FIGURE 8. Antenna configurations of the compact design of the proposed 2 × 2 MIMO antenna set: (a) perspective view, (b) side view, and (c) simulated S-parameters.

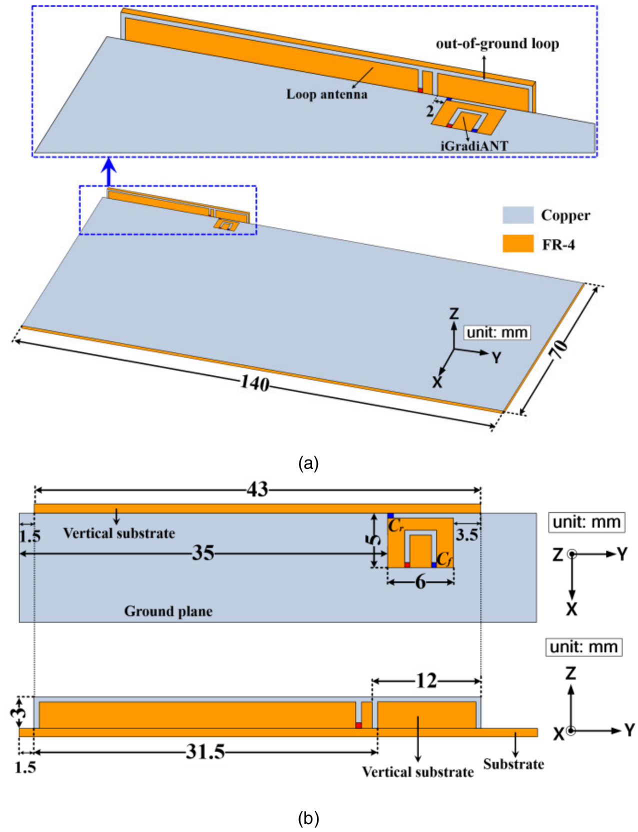

FIGURE 9. Integration of iGradiANT and a loop antenna: (a) perspective view, and (b) side view.

and the iGradiANT are assembled without any separation. In this design, the loop antenna and the out-of-ground loop are disposed of in the same 0.8-mm-thick FR4 substrate. The loop antenna is a one-wavelength resonator whose perimeter is usually one wavelength. As shown, the loop antenna has a dimension of 3 mm × 31.5 mm, and the overall dimension of the vertically implemented FR4 substrate is 3 mm × 43 mm × 0.8 mm. More information on the dimensions can be found in Fig. 9.

Figure 10 presents the simulated S-parameters of the integrated MIMO antenna set composed of the iGradiANT and the loop antenna. It can be observed that the port-to-port isolation between the iGradiANT and the loop antenna is higher than 16 dB, and the produced impedance bandwidths can sufficiently cover the target frequency band for the sub-6 GHz applications. On the contrary, the reference MIMO antenna set without using the out-of-ground loop (the loop antenna and the conventional GradiANT) suffers from severe mutual coupling as high as −8 dB, as shown in Fig. 10 (b). Therefore, the proposed iGradiANT is also compatible with a normal loop antenna, consisting of another integrated MIMO antenna set with inherent isolation, which demonstrates the feasibility and versatility of the proposed technique. Note that the decoupling effect can be improved if properly adjusting the connection portion between the out-of-ground loop and the loop antenna while simultaneously tuning the parameters discussed in Section III-B.

Accordingly, some exciting and relevant conclusions can be extracted:

a) In contrast to a traditional GradiANT, the proposed iGradiANT exploits an out-of-ground loop and produces an anti-phase current mode to produce inherent isolation with the adjacent antenna element;

b) The isolation level between the iGradiANT and the adjacent antenna element can be conveniently controlled by modifying the electrical length of the out-of-ground loop;

c) The iGradiANT-based MIMO antenna set advantages in high integration, high isolation, convenient control, and easy fabrication.

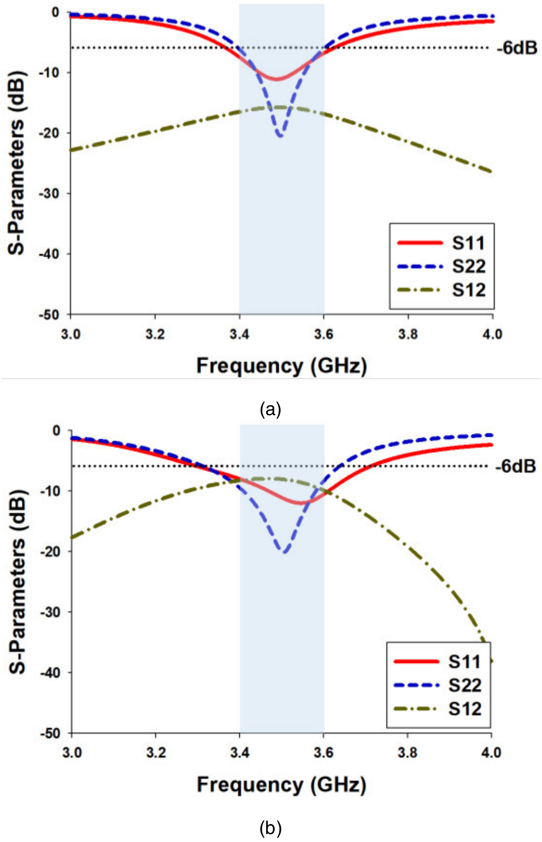

FIGURE 10. Simulated S-parameters: (a) Integration of iGradANT and the loop antenna, and (b) the reference MIMO antenna set (without the out-of-ground loop).

More research is under study. For example, it is desirable to investigate various integration methods of the iGradiANT with various types of antenna elements; iGradiANT in the metal-rimmed terminal devices is an interesting and imperative task to carry on; moreover, a comprehensive analysis of the interaction between the iGradiANT and its implementation circumstances, including handset effects (such as chassis, metallic components), and user scenarios, is on-going.

IV. DEMONSTRATION OF 8 × 8 MIMO ANTENNA ARRAY

The proposed 2 × 2 MIMO antenna set can be easily duplicated to construct 4 × 4 and 8 × 8 MIMO antenna arrays in current and future 5G terminal devices, satisfying the desperate request for increasing antenna elements for the usage of 5G applications. As a case study, an 8 × 8 MIMO antenna array is presented in Fig. 11, where four sets of the proposed 2 × 2 MIMO antenna set (Module 1, Module 2, Module 3, and Module 4) are symmetrically implemented along the long sides of the ground plane. It noted that the dimensions of each 2 × 2 MIMO set are the same as those in Fig. 2, and more information can be found in Fig. 11. Furthermore, the prototype of the fabricated 8 × 8 MIMO antennas is pictured in Fig. 12, where eight 50 Ω semirigid cables with equal lengths are used to feed the antennas; measurement was then conducted to further validate the feasibility of the proposed 8 × 8 MIMO antenna array.

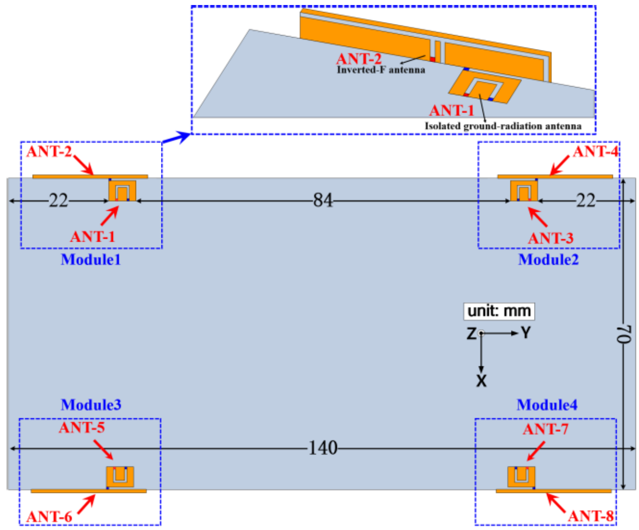

FIGURE 11. Antenna configurations of the proposed 8 × 8 MIMO antenna array.

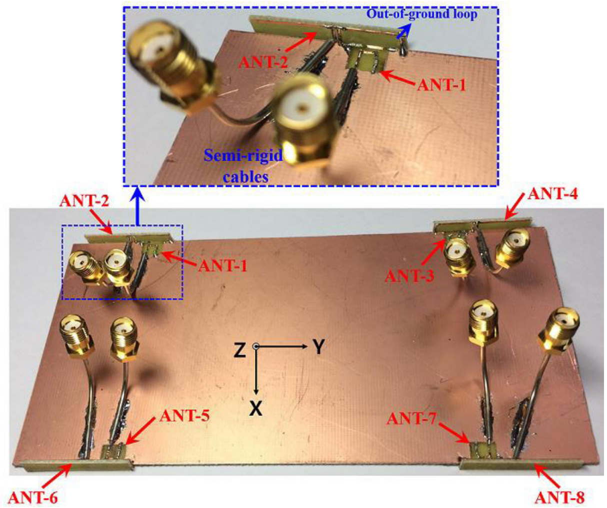

FIGURE 12. The prototype of the fabricated 8 × 8 MIMO antennas.

The simulated and measured S-parameters of the proposed 8 × 8 MIMO antenna array are plotted in Fig. 13, where only S_{11} and S_{22} curves are given due to the structural symmetry. It can be observed in Fig. 13(a) that the 3:1 VSWR bandwidths of Antenna 1 (iGradiANT) and Antenna 2 (IFA) in simulation are 270 MHz (from 3.38 to 3.65 GHz) and 260 MHz (from 3.38 to 3.64 GHz), respectively, sufficiently covering the 3.5 GHz target frequency band. As can be verified from Figs. 13(b) and 13(c), the proposed MIMO antennas exhibit high isolation properties between each two antenna elements. Minimum isolation (above 14 dB) in simulation is generated between Antenna 1 and Antenna 3 (see the S_{13} curve), and maximum isolation (above 26 dB) can be observed between Antenna 1 and Antenna 8 (see the S_{18} curve). As can be observed, the measured results agree well with the simulated results; the minor discrepancy may be attributed to the fabrication error and the surface current induced on the outer surface of the outer conductor of

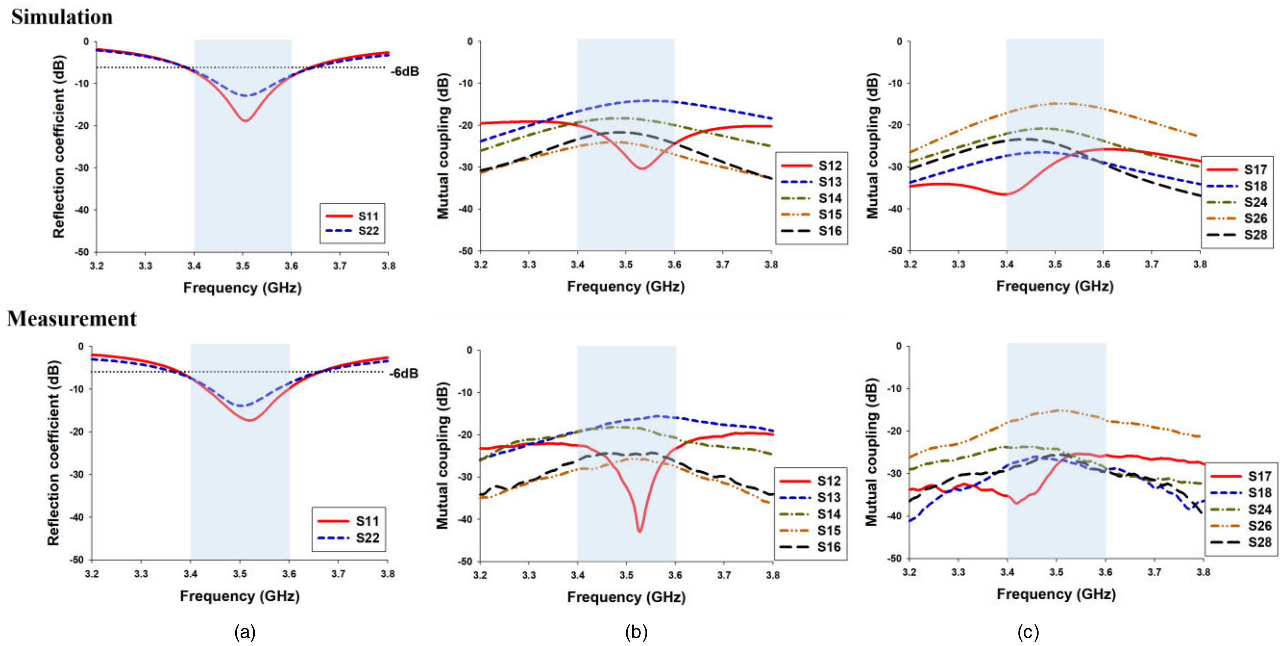

FIGURE 13. Simulated and measured S-parameters of the proposed 8 × 8 MIMO antenna array: (a) reflection coefficients, (b), and (c) mutual coupling.

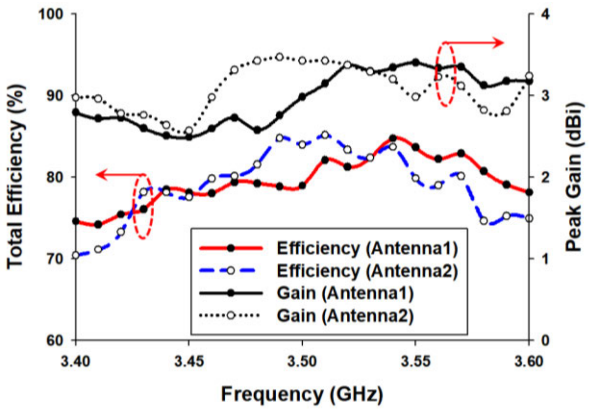

FIGURE 14. Measured total efficiencies and peak gains of the proposed 8 × 8 MIMO antennas.

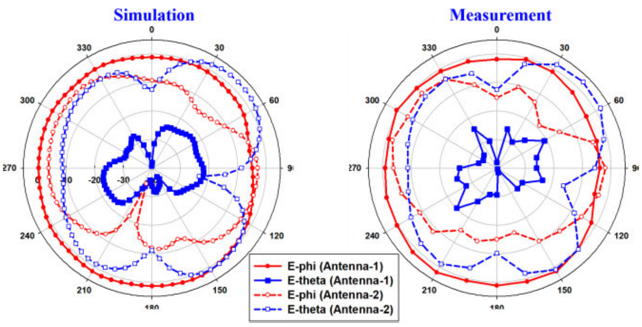

FIGURE 15. Simulated and measured radiation patterns of the proposed 8 × 8 MIMO antenna array in the *xz*-plane at 3.5 GHz.

attached semirigid cables. It is noted that ideal components are modeled in simulation, while high-Q capacitors are utilized in measurement to avoid any undesired effect. Hence, the proposed 8 × 8 MIMO antenna array can fully cover the 3.5 GHz operating frequency band and produce high isolation above 15 dB between any two antenna elements, indicating the feasibility of the proposed technique for 5G MIMO applications. Therefore, the proposed 8 × 8 MIMO antenna array can be a promising candidate for the applications of 5G terminal devices.

The fabricated 8 × 8 MIMO antennas are then measured in a 6 m × 3 m × 3 m three-dimensional (3D) CTIA OTA anechoic chamber to compute its far-field characteristics. The measured total radiation efficiencies and peak gains are shown in Fig. 14, where the radiation efficiencies and gains of both antennas are over 70% and 2.5 dBi, respectively, indicating their high radiation performance and practicability in practical scenarios.

The simulated and measured radiation patterns in the *xz*-plane generated by Antenna-1 and Antenna-2 are displayed in Fig. 15 to validate the diversity performance of the proposed MIMO antenna array. The $\boldsymbol{E}_{\varphi}$ component is omnidirectional for Antenna-1 while having radiation nulls for Antenna-2. On the other hand, the $\boldsymbol{E}_{\theta}$ component of Antenna-2 is much stronger than that of Antenna-1. Therefore, this polarization difference between Antenna-1 and Antenna-2 determines their diversity performance.

The envelope correlation coefficient (ECC) ρ_e is a critical figure-of-merit to evaluate the diversity performance of a MIMO antenna system, which can be derived by calculating the vector properties (magnitude, phase, and polarization) of the complex fields, as follows

$$\rho_e = \frac{\left| \iint_{4\pi} \left[\vec{F}_1(\theta, \phi) \vec{F}_2(\theta, \phi) \right] d\Omega \right|^2}{\iint_{4\pi} \left| \vec{F}_1(\theta, \phi) \right|^2 d\Omega \iint_{4\pi} \left| \vec{F}_2(\theta, \phi) \right|^2 d\Omega} \tag{1}$$

TABLE 1. Comparisons with previously published literature.

Ref.	Decoupling method	Array scale	Minimum spacing	-6dB impedance bandwidth	Isolation	Measured efficiency (peak gain)	Complexity
[5]	Self-decoupled	8 × 8	Integrated	>200 MHz	>10 dB	>40% (not shown)	Complicated try-and-error process
[9] [12]	Self-decoupled	8 × 8	Integrated	>200 MHz	>18 dB	>47% (>1.15 dBi)	Need for large clearance area
[11]	Self-decoupled	4 × 4 or 8 × 8	Integrated	>200 MHz	>17 dB	>49% (not shown)	Difficult installation
[13]	Self-decoupled	4 × 4 or 8 × 8	Integrated	>200 MHz	>12.9 dB	>37.7% (not shown)	Need for large clearance area and complex matching networks
[14]	Self-decoupled	8 × 8	Integrated	600 MHz	>15 dB	>60% (~5 dBi)	Need for a large area in the system ground
[18]	Decoupling structure	8 × 8	17 mm	>300 MHz	>15 dB	>45% (>2 dBi)	Complex
[20]	Decoupling structure	8 × 8	30 mm	>200MHz	>20 dB	>38% (not shown)	Need for large-sized decoupling structure
[29]	Spatial arrangement	8 × 8	17 mm	>200MHz	>10 dB	>62% (>1.9 dBi)	Simple
[32]	Decoupling network	8 × 8	< 5 mm	>135 MHz	>11.6 dB	>20% (not shown)	Difficult installation
This work	Self-decoupled	8 × 8	Integrated	>270 MHz	>14 dB	>70% (>2.5 dBi)	Simple

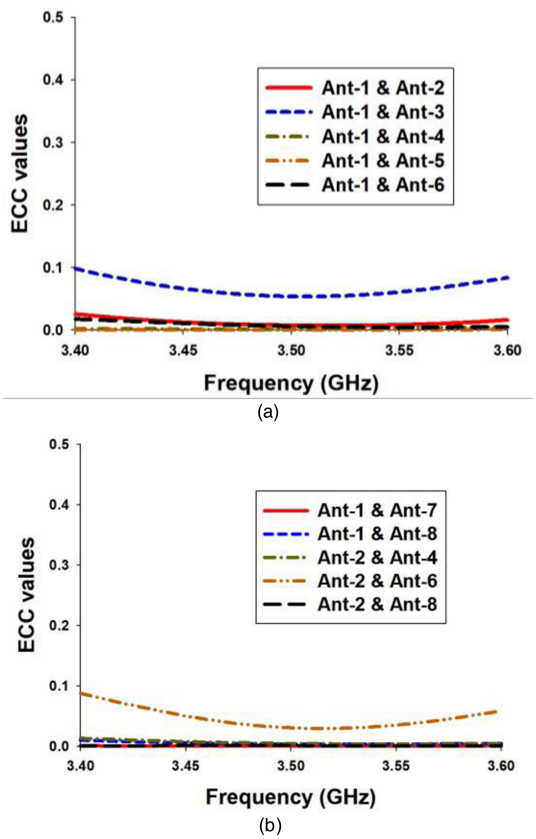

FIGURE 16. Measured ECC values of the proposed 8 × 8 MIMO antenna array.

where $\vec{F}_i(\theta, \phi)$ is the field radiation pattern of the antenna when port i is excited [64]. Accordingly, the computed results based on measured radiation patterns are presented in Fig. 16, and it can be verified that the ECC values between any two antennas are below 0.1, which is much lower than the acceptance criteria in mobile communications ($\rho_e < 0.5$) [64]. Therefore, it can be concluded that the proposed technique provides not only high isolation (low mutual coupling) but also low correlation performance, satisfying current and future 5G MIMO applications.

Finally, a comparison with the state-of-the-art literature is presented in Table 1 to clarify the novelty of the proposed technique. As can be observed, decoupling techniques using decoupling structures, spatial arrangement, and decoupling networks, suffer from large spatial distances or need for complex decoupling processes and structures. On the contrary, self-decoupled techniques can achieve integrated and compact MIMO antenna arrays. Compared to previously reported self-decoupled MIMO antenna arrays, this work can provide comparative impedance bandwidth and isolation property; more importantly, the proposed technique has superiority in high radiation performance, simple integration, and versatile compatibility.

V. CONCLUSION

A novel iGradiANT with inherent isolation to the adjacent antenna element is proposed in the first of its kind, allowing the successful accomplishment of a compact MIMO antenna set for 5G MIMO applications. The proposed iGradiANT is featured in its unique structure of the out-of-ground loop and fundamental characteristic of two anti-phase loop-type current modes. It has been verified that both a typically used IFA and a normal loop antenna can be separately combined with the iGradiANT, forming integrated 2 × 2 MIMO antenna sets without any separation. High isolation is obtained within the overall operating band, which is attributed to the near-field energy cancellation between the out-of-ground current mode and in-ground current mode; thus, optimized results can be derived by merely manipulating the dimension of the out-of-ground loop. An 8 × 8 MIMO antenna array is presented in both simulation and measurement for the usage of current and future 5G applications. In measurement, a minimum isolation level above 15 dB can be obtained between each two antenna elements, and the ECC values are all below 0.1. Therefore, the proposed MIMO antenna array, having the advantages of compactness, convenient control, high isolation, and low correlation, can be applied for current and future 5G MIMO applications.

REFERENCES

[1] F. Boccardi, R. W. Heath, A. Lozano, T. L. Marzetta, and P. Popovski, "Five disruptive technology directions for 5G," *IEEE Commun. Mag.*, vol. 52, no. 2, pp. 74–80, Feb. 2014.

[2] M. Agiwal, A. Roy, and N. Saxena, "Next generation 5G wireless networks: A comprehensive survey," *IEEE Commun. Surveys Tuts.*, vol. 18, no. 3, pp. 1617–1655, 3rd Quart., 2016.

[3] WRC-15 Press Release. (Nov. 27, 2015). *World Radiocommunication Conference Allocates Spectrum for Future Innovation*. [Online]. Available: http://www.itu.int/net/pressoffice/press_releases/2015/56.aspx

[4] K.-L. Wong, B.-W. Lin, and B. W.-Y. Li, "Dual-band dual inverted-F/loop antennas as a compact decoupled building block for forming eight 3.5/5.8-GHz MIMO antennas in the future smartphone," *Microw. Opt. Technol. Lett.*, vol. 59, no. 11, pp. 2715–2721, Nov. 2017.

[5] K.-L. Wong, C.-Y. Tsai, and J.-Y. Lu, "Two asymmetrically mirrored gap-coupled loop antennas as a compact building block for eight-antenna MIMO array in the future smartphone," *IEEE Trans. Antennas Propag.*, vol. 65, no. 4, pp. 1765–1778, Apr. 2017.

[6] C.-Y. Tsai, K.-L. Wong, and W.-Y. Li, "Experimental results of the multi-gbps smartphone with 20 multi-input multi-output (MIMO) antennas in the 20 × 12 MIMO operation," *Microw. Opt. Technol. Lett.*, vol. 60, no. 8, pp. 2001–2010, Aug. 2018.

[7] Z. Ren, A. Zhao, and S. Wu, "MIMO antenna with compact decoupled antenna pairs for 5G mobile terminals," *IEEE Antennas Wireless Propag. Lett.*, vol. 18, no. 7, pp. 1367–1371, Jul. 2019.

[8] Z. Ren and A. Zhao, "Dual-band MIMO antenna with compact self-decoupled antenna pairs for 5G mobile applications," *IEEE Access*, vol. 7, pp. 82288–82296, 2019.

[9] A. Ren, Y. Liu, H.-W. Yu, Y. Jia, C.-Y.-D. Sim, and Y. Xu, "A high-isolation building block using stable current nulls for 5G smartphone applications," *IEEE Access*, vol. 7, pp. 170419–170429, 2019.

[10] C.-Z. Han, L. Xiao, Z. Chen, and T. Yuan, "Co-located self-neutralized handset antenna pairs with complementary radiation patterns for 5G MIMO applications," *IEEE Access*, vol. 8, pp. 73151–73163, 2020.

[11] L. Sun, H. Feng, Y. Li, and Z. Zhang, "Compact 5G MIMO mobile phone antennas with tightly arranged orthogonal-mode pairs," *IEEE Trans. Antennas Propag.*, vol. 66, no. 11, pp. 6364–6369, Nov. 2018.

[12] A. Ren, Y. Liu, and C.-Y.-D. Sim, "A compact building block with two shared-aperture antennas for eight-antenna MIMO array in metal-rimmed smartphone," *IEEE Trans. Antennas Propag.*, vol. 67, no. 10, pp. 6430–6438, Oct. 2019.

[13] L. Chang, Y. Yu, K. Wei, and H. Wang, "Polarization-orthogonal co-frequency dual antenna pair suitable for 5G MIMO smartphone with metallic bezels," *IEEE Trans. Antennas Propag.*, vol. 67, no. 8, pp. 5212–5220, Aug. 2019.

[14] N. O. Parchin, Y. I. A. Al-Yasir, A. H. Ali, I. Elfergani, J. M. Noras, J. Rodriguez, and R. A. Abd-Alhameed, "Eight-element dual-polarized MIMO slot antenna system for 5G smartphone applications," *IEEE Access*, vol. 7, pp. 15612–15622, 2019.

[15] M.-Y. Li, Z.-Q. Xu, Y.-L. Ban, C.-Y.-D. Sim, and Z.-F. Yu, "Eight-port orthogonally dual-polarised MIMO antennas using loop structures for 5G smartphone," *IET Microw., Antennas Propag.*, vol. 11, no. 12, pp. 1810–1816, Sep. 2017.

[16] K.-L. Wong, J.-Y. Lu, L.-Y. Chen, W.-Y. Li, and Y.-L. Ban, "8-antenna and 16-antenna arrays using the quad-antenna linear array as a building block for the 3.5-GHz LTE MIMO operation in the smartphone," *Microw. Opt. Technol. Lett.*, vol. 58, no. 1, pp. 174–181, Jan. 2016.

[17] J. Guo, L. Cui, C. Li, and B. Sun, "Side-edge frame printed eight-port dual-band antenna array for 5G smartphone applications," *IEEE Trans. Antennas Propag.*, vol. 66, no. 12, pp. 7412–7417, Dec. 2018.

[18] W. Jiang, B. Liu, Y. Cui, and W. Hu, "High-isolation eight-element MIMO array for 5G smartphone applications," *IEEE Access*, vol. 7, pp. 34104–34112, 2019.

[19] Y. Li, C.-Y.-D. Sim, Y. Luo, and G. Yang, "Metal-frame-integrated eight-element multiple-input multiple-output antenna array in the long term evolution bands 41/42/43 for fifth generation smartphones," *Int. J. RF Microw. Comput.-Aided Eng.*, vol. 29, no. 1, Jan. 2019, Art. no. e21495.

[20] H. Xu, H. Zhou, S. Gao, H. Wang, and Y. Cheng, "Multimode decoupling technique with independent tuning characteristic for mobile terminals," *IEEE Trans. Antennas Propag.*, vol. 65, no. 12, pp. 6739–6751, Dec. 2017.

[21] L. Cui, J. Guo, Y. Liu, and C.-Y.-D. Sim, "An 8-element dual-band MIMO antenna with decoupling stub for 5G smartphone applications," *IEEE Antennas Wireless Propag. Lett.*, vol. 18, no. 10, pp. 2095–2099, Oct. 2019.

[22] W. Jiang, Y. Cui, B. Liu, W. Hu, and Y. Xi, "A dual-band MIMO antenna with enhanced isolation for 5G smartphone applications," *IEEE Access*, vol. 7, pp. 112554–112563, Aug. 2019.

[23] A. A. Al-Hadi, J. Ilvonen, R. Valkonen, and V. Viikari, "Eight-element antenna array for diversity and MIMO mobile terminal in LTE 3500 MHz band," *Microw. Opt. Technol. Lett.*, vol. 56, no. 6, pp. 1323–1327, Jun. 2014.

[24] M.-Y. Li, Y.-L. Ban, Z.-Q. Xu, G. Wu, C.-Y.-D. Sim, K. Kang, and Z.-F. Yu, "Eight-port orthogonally dual-polarized antenna array for 5G smartphone applications," *IEEE Trans. Antennas Propag.*, vol. 64, no. 9, pp. 3820–3830, Sep. 2016.

[25] Y. Li, C.-Y.-D. Sim, Y. Luo, and G. Yang, "12-port 5G massive MIMO antenna array in sub-6GHz mobile handset for LTE bands 42/43/46 applications," *IEEE Access*, vol. 6, pp. 344–354, 2018.

[26] X. Zhang, Y. Li, W. Wang, and W. Shen, "Ultra-wideband 8-port MIMO antenna array for 5G metal-frame smartphones," *IEEE Access*, vol. 7, pp. 72273–72282, 2019.

[27] Y. Li, C.-Y.-D. Sim, Y. Luo, and G. Yang, "High-isolation 3.5 GHz eight-antenna MIMO array using balanced open-slot antenna element for 5G smartphones," *IEEE Trans. Antennas Propag.*, vol. 67, no. 6, pp. 3820–3830, Jun. 2019.

[28] Y.-L. Ban, C. Li, C.-Y.-D. Sim, G. Wu, and K.-L. Wong, "Multiband 10-antenna array for sub-6 GHz MIMO applications in 5-G smartphones," *IEEE Access*, vol. 4, pp. 2981–2988, 2019.

[29] Y. Li, C.-Y.-D. Sim, Y. Luo, and G. Yang, "4G/5G multiple antennas for future multi-mode smartphone applications," *IEEE Access*, vol. 6, pp. 28041–28053, 2019.

[30] Y. Liu, A. Ren, H. Liu, H. Wang, and C.-Y.-D. Sim, "Eight-port MIMO array using characteristic mode theory for 5G smartphone applications," *IEEE Access*, vol. 7, pp. 45679–45692, 2019.

[31] M.-Y. Li, Y.-L. Ban, Z.-Q. Xu, J. Guo, and Z.-F. Yu, "Tri-polarized 12-antenna MIMO array for future 5G smartphone applications," *IEEE Access*, vol. 6, pp. 6160–6170, 2018.

[32] C. Deng, D. Liu, and X. Lv, "Tightly arranged four-element MIMO antennas for 5G mobile terminals," *IEEE Trans. Antennas Propag.*, vol. 67, no. 10, pp. 6353–6361, Oct. 2019.

[33] J. Andersen and H. Rasmussen, "Decoupling and descattering networks for antennas," *IEEE Trans. Antennas Propag.*, vol. AP-24, no. 6, pp. 841–846, Nov. 1976.

[34] S.-C. Chen, Y.-S. Wang, and S.-J. Chung, "A decoupling technique for increasing the port isolation between two strongly coupled antennas," *IEEE Trans. Antennas Propag.*, vol. 56, no. 12, pp. 3650–3658, Dec. 2008.

[35] L. Zhao, L. K. Yeung, and K.-L. Wu, "A coupled resonator decoupling network for two-element compact antenna arrays in mobile terminals," *IEEE Trans. Antennas Propag.*, vol. 62, no. 5, pp. 2767–2776, May 2014.

[36] L. Zhao and K.-L. Wu, "A dual-band coupled resonator decoupling network for two coupled antennas," *IEEE Trans. Antennas Propag.*, vol. 63, no. 7, pp. 2843–2850, Jul. 2015.

[37] Y. Chen and D. Manteuffel, "A tunable decoupling and matching concept for compact mobile terminal antennas," *IEEE Trans. Antennas Propag.*, vol. 65, no. 4, pp. 1570–1578, Apr. 2017.

[38] A. Diallo, C. Luxey, P. Le Thuc, R. Staraj, and G. Kossiavas, "Study and reduction of the mutual coupling between two mobile phone PIFAs operating in the DCS1800 and UMTS bands," *IEEE Trans. Antennas Propag.*, vol. 54, no. 11, pp. 3063–3074, Nov. 2006.

[39] A. Diallo, C. Luxey, P. Le Thuc, R. Staraj, and G. Kossiavas, "Enhanced two-antenna structures for UMTS diversity terminals," *Microw., Antennas Propag.*, vol. 2, no. 1, pp. 93–101, Feb. 2008.

[40] S.-W. Su, C.-T. Lee, and F.-S. Chang, "Printed MIMO-antenna system using neutralization-line technique for wireless USB-dongle applications," *IEEE Trans. Antennas Propag.*, vol. 60, no. 2, pp. 456–463, Feb. 2012.

[41] Y. Wang and Z. Du, "A wideband printed dual-antenna with three neutralization lines for mobile terminals," *IEEE Trans. Antennas Propag.*, vol. 62, no. 3, pp. 1495–1500, Mar. 2014.

[42] K.-L. Wong and L.-Y. Chen, "Dual-inverted-F antenna with a decoupling chip inductor for the 3.6-GHz LTE operation in the tablet computer," *Microw. Opt. Technol. Lett.*, vol. 57, no. 9, pp. 2189–2194, Sep. 2015.

[43] C.-Y. Chiu, C.-H. Cheng, R. D. Murch, and C. R. Rowell, "Reduction of mutual coupling between closely-packed antenna elements," *IEEE Trans. Antennas Propag.*, vol. 55, no. 6, pp. 1732–1738, Jun. 2007.

[44] A. C. K. Mak, C. R. Rowell, and R. D. Murch, "Isolation enhancement between two closely packed antennas," *IEEE Trans. Antennas Propag.*, vol. 56, no. 11, pp. 3411–3419, Nov. 2008.

[45] C.-C. Hsu, K.-H. Lin, and H.-L. Su, "Implementation of broadband isolator using metamaterial-inspired resonators and a T-shaped branch for MIMO antennas," *IEEE Trans. Antennas Propag.*, vol. 59, no. 10, pp. 3936–3939, Oct. 2011.

[46] B. K. Lau and J. B. Andersen, "Simple and efficient decoupling of compact arrays with parasitic scatterers," *IEEE Trans. Antennas Propag.*, vol. 60, no. 2, pp. 464–472, Feb. 2012.

[47] Z. Li, Z. Du, M. Takahashi, K. Saito, and K. Ito, "Reducing mutual coupling of MIMO antennas with parasitic elements for mobile terminals," *IEEE Trans. Antennas Propag.*, vol. 60, no. 2, pp. 473–481, Feb. 2012.

[48] H. T. Chattha, Y. Huang, S. J. Boyes, and X. Zhu, "Polarization and pattern diversity-based dual-feed planar Inverted-F antenna," *IEEE Trans. Antennas Propag.*, vol. 60, no. 3, pp. 1532–1539, Mar. 2012.

[49] H. Li, B. K. Lau, Z. Ying, and S. He, "Decoupling of multiple antennas in terminals with chassis excitation using polarization diversity, angle diversity and current control," *IEEE Trans. Antennas Propag.*, vol. 60, no. 12, pp. 5947–5957, Dec. 2012.

[50] B. Kim, Y. Park, H. Wi, M.-J. Park, Y. Choi, J. Lee, W. Jung, D. Kim, and B. Lee, "Isolation enhancement of USB dongle MIMO antenna in LTE 700 band applications," *IEEE Antennas Wireless Propag. Lett.*, vol. 11, pp. 961–964, Aug. 2012.

[51] K. K. Kishor and S. V. Hum, "A two-port chassis-mode MIMO antenna," *IEEE Antennas Wireless Propag. Lett.*, vol. 12, pp. 690–693, 2013.

[52] R. Martens and D. Manteuffel, "Systematic design method of a mobile multiple antenna system using the theory of characteristic modes," *IET Microw., Antennas Propag.*, vol. 8, no. 12, pp. 887–893, Sep. 2014.

[53] L. Qu, J. Jeon, D. Park, and H. Kim, "Antenna design based on quasi-degenerate characteristic modes of unbroken metal rim," *IET Microw., Antennas Propag.*, vol. 11, no. 15, pp. 2168–2173, Dec. 2017.

[54] Y. Liu, H. H. Kim, J. Lee, and H. Kim, "Ground radiation method using slot with coupling capacitors," *Electron. Lett.*, vol. 49, no. 7, pp. 447–448, Mar. 2013.

[55] Y. Liu, H.-H. Kim, and H. Kim, "Loop-type ground radiation antenna for dual-band WLAN applications," *IEEE Trans. Antennas Propag.*, vol. 61, no. 9, pp. 4819–4823, Sep. 2013.

[56] L. Qu, R. Zhang, and H. Kim, "High-sensitivity ground radiation antenna system using an adjacent slot for Bluetooth headsets," *IEEE Trans. Antennas Propag.*, vol. 63, no. 12, pp. 5903–5907, Dec. 2015.

[57] L. Qu, H. Kim, and R. Zhang, "Decoupling between ground radiation antennas with ground-coupled loop-type isolator for WLAN applications," *IET Microw., Antennas Propag.*, vol. 10, no. 5, pp. 546–552, Apr. 2016.

[58] L. Qu, Z. Zahid, H.-H. Kim, and H. Kim, "Circular polarized ground radiation antenna for mobile applications," *IEEE Trans. Antennas Propag.*, vol. 66, no. 5, pp. 2655–2660, May 2018.

[59] L. Qu, H. Piao, Y. Qu, H.-H. Kim, and H. Kim, "Circularly polarised MIMO ground radiation antennas for wearable devices," *Electron. Lett.*, vol. 54, no. 4, pp. 189–190, Feb. 2018.

[60] W. Lei, H. Chu, and Y.-X. Guo, "Design of a circularly polarized ground radiation antenna for biomedical applications," *IEEE Trans. Antennas Propag.*, vol. 64, no. 6, pp. 2535–2540, Jun. 2016.

[61] Y.-F. Lin, M.-J. Chang, H.-M. Chen, and S.-T. Huang, "Theoretical study of ground radiation tag antenna with tunable open-slot exciter," *Int. J. Microw. Wireless Technol.*, vol. 9, no. 4, pp. 945–952, May 2017.

[62] Z. Zahid and H. Kim, "Analysis of a loop type ground radiation antenna based on equivalent circuit model," *IET Microw., Antennas Propag.*, vol. 11, no. 1, pp. 23–28, Jan. 2017.

[63] H. Piao and L. Qu, "An isolated ground-radiation antenna and its MIMO antenna systems," CN Patent 201 911 244 425.6, Dec. 6, 2019.

[64] R. G. Vaughan and J. B. Andersen, "Antenna diversity in mobile communications," *IEEE Trans. Veh. Technol.*, vol. VT-36, no. 4, pp. 149–172, Nov. 1987.